Over 20% ^{13}C Hyperpolarization for Pyruvate Using Deuteration and Rapid SLIC-SABRE in Mictrotesla Fields

Andreas B. Schmidt,*[a,b,c] James Eills,[d] Laurynas Dagys,[e] Martin Gierse,[e] Michael Keim,[e] Sebastian Lucas,[e] Michael Bock,[a] Ilai Schwartz,[e] Maxim Zaitsev,[a] Eduard Y. Chekmenev,[c,f] Stephan Knecht*[e]

[a] Dr. A. B. Schmidt, Prof. Dr. Michael Bock, Prof. Dr. Maxim Zaitsev
Division of Medical Physics, Department of Radiology, Medical Center, Faculty of Medicine,
University of Freiburg, Killianstr. 5a, Freiburg 79106, Germany
E-Mail: andreas.schmidt@uniklinik-freiburg.de

[b] Dr. A. B. Schmidt
German Cancer Consortium (DKTK), partner site Freiburg and German Cancer Research Center (DKFZ),
Im Neuenheimer Feld 280, Heidelberg 69120, Germany

[c] Dr. A. B. Schmidt, Prof. Dr. E. Y. Chekmenev
Department of Chemistry, Integrative Biosciences (Ibio), Karmanos CancerInstitute (KCI),
Wayne State University, Detroit, Michigan 48202, United States

[d] Dr. J. Eills
Institute for Bioengineering of Catalonia, Barcelona Institute of Science and Technology, 08028 Barcelona, Spain

[e] Dr. L. Dagys, M. Gierse, M. Keim, S. Lucas, I. Schwartz, Dr. S. Knecht
NVision Imaging Technologies GmbH, 89081 Ulm, Germany
E-mail: stephan@nvision-imaging.com

[f] Prof. Dr. E. Y. Chekmenev
Russian Academy of Sciences (RAS)
14 Leninskiy Prospekt, 119991 Moscow, Russia

Abstract: Carbon-13 hyperpolarized pyruvate is about to become the next-generation contrast agent for molecular magnetic resonance imaging of cancer and other diseases. Here, efficient and rapid pyruvate hyperpolarization is achieved via Signal Amplification by Reversible Exchange (SABRE) with parahydrogen through synergistic use of substrate deuteration, alternating, and static microtesla magnetic fields. Up to 22% and 6% long-lasting ^{13}C polarization (T_1=3.7±0.25min and T_1=1.7±0.1min) is demonstrated for the C1 and C2 nuclear sites, respectively. The remarkable polarization levels become possible due to favorable relaxation dynamics at the microtesla fields. The ultra-long polarization lifetimes will be conducive to yielding high polarization after purification, quality assurance, and injection of the hyperpolarized molecular imaging probes. These results pave the way to future in vivo translation of carbon-13 hyperpolarized molecular imaging probes prepared by this approach.

Hyperpolarized (HP) ^{13}C-pyruvate is being used as a contrast agent in clinical trials, since its metabolic flux can be tracked noninvasively and temporally resolved using magnetic resonance imaging (MRI).[1] This carries valuable diagnostic information, since abnormal pyruvate metabolism is associated with various pathologies (e.g., tumour cells exhibit accelerated pyruvate-to-lactate conversion; "Warburg effect").[2] Pyruvate has emerged as the leading HP MRI agent because of fast cellular uptake and its central position in cellular metabolism at the cross-section of glycolysis, the citric acid cycle, alanine transamination, and lactate fermentation.[3] HP pyruvate is under evaluation in over 30 clinical trials as off 2022. In almost all cases [1-^{13}C]pyruvate is used, but [2-^{13}C]pyruvate has recently been demonstrated in humans with the advantage that the C2 atom enters the citric acid cycle.[4] The leading technology for HP pyruvate is dissolution dynamic nuclear polarization (dDNP).[5] However, it is expensive (~2M€) and low throughput (~1hour per sample). More cost effective and faster technologies are needed for future widespread clinical utilization.

Duckett and coworkers have pioneered a "non-hydrogenative" parahydrogen- (pH_2-) based hyperpolarization approach referred to as signal amplification by reversible exchange (SABRE).[6–8] It relies on reversible, simultaneous binding of pH_2, which is the nuclear spin-singlet isomer of molecular hydrogen, and the target molecule to an iridium-based exchange complex.[9] Recently, SABRE was used to produce HP pyruvate,[10] with P_{13C}≈10% for [1-^{13}C]pyruvate and P_{13C}≈1% for [2-^{13}C]pyruvate.[11,12] In another important step, the extraction of highly polarized (P_{13C}≈9%) [1-^{13}C]pyruvate into aqueous solution after precipitation from methanol was shown, paving the way to future biomedical MRI studies with SABRE-polarized pyruvate.[13]

In SABRE, polarization transfer from pH_2 to ^{13}C is mediated by the indirect dipolar couplings (J-couplings) between nuclei in the transient complexes 2 and 2' shown in Fig. 1b. For SABRE, the ultralow magnetic field regime (hundreds of nanotesla) plays an important role. At these fields, nuclear spin energy states of the molecules are matching and the J-coupling interaction effectively perturbs the eigenstates such that energy level crossing is avoided (level anti crossing, LAC).[14] When a SABRE reaction is carried out at the LAC, the target ^{13}C spin is spontaneously hyperpolarized.[15–17] This method is called SABRE-SHEATH (SABRE in shield enables alignment transfer to heteronuclei), and has been demonstrated for [1-^{13}C]pyruvate. More recently, pulsed static fields have been used to induce this effect, delivering similar ^{13}C polarization (P_{13C}) of HP [1-^{13}C]pyruvate as SABRE-SHEATH.[18–21] Pulsed radiofrequency (rf) fields can be employed for polarization transfer.[22,23] Spin-lock induced crossing (SLIC) by continuous rf irradiation at tesla fields has

also been applied along with SABRE and was termed low-irradiation generation of high tesla- (LIGHT-) or SLIC-SABRE.[24–28] However, P_{13C} achieved by high-field SLIC-SABRE were found to be lower than those obtained via SABRE-SHEATH. The reason for these low P_{13C} is that SLIC at tesla fields faces significant challenges: often unfavourable relaxation dynamics because of chemical shift anisotropy (CSA), singlet-to-triplet mixing of parahydrogen,[29] and a need for selective excitation of the bound and free SABRE species due to larger chemical shift dispersion. In sharp contrast, at microtesla fields, ^{13}C chemical shift differences are negligible and relaxation times become favorable.

Here we show that SLIC-SABRE can be carried out at microtesla fields to quickly hyperpolarize [1-^{13}C]- and [2-^{13}C]pyruvate-d_3, producing high ^{13}C polarizations of P_{13C} = 22% and P_{13C} = 6%, respectively (Fig. 1a). Compared to the thermal equilibrium polarization of $P_{13C} \approx 0.0002\%$ at the 1.9 T detection field, these P_{13C} levels correspond to signal enhancements of 140,000- and 40,000-fold. To achieve these P_{13C} levels, we performed the SABRE reaction (Fig. 1b) by bubbling pH_2 through a solution of ~30mM pyruvate-d_3 in CD_3OD at 50μT and at ~3-7°C (Fig. 1c) in the presence of a spin-lock induced crossing (SLIC) rf field (Fig. 1d). Pyruvate-d_3 (and pyruvate-h_3 below) was used with natural ^{13}C abundance (1.1%) to minimize sample-to-sample variability; no difference in P_{13C} values between ^{13}C-labeled and natural-abundance samples was observed. After the SLIC process, an adiabatic 90° pulse was used to align the ^{13}C polarization longitudinally along the 50 μT field, and the sample was moved from the SABRE setup to an 80MHz benchtop NMR system for HP ^{13}C signal acquisition. A detailed description of the setup and methods is reported in the SI.

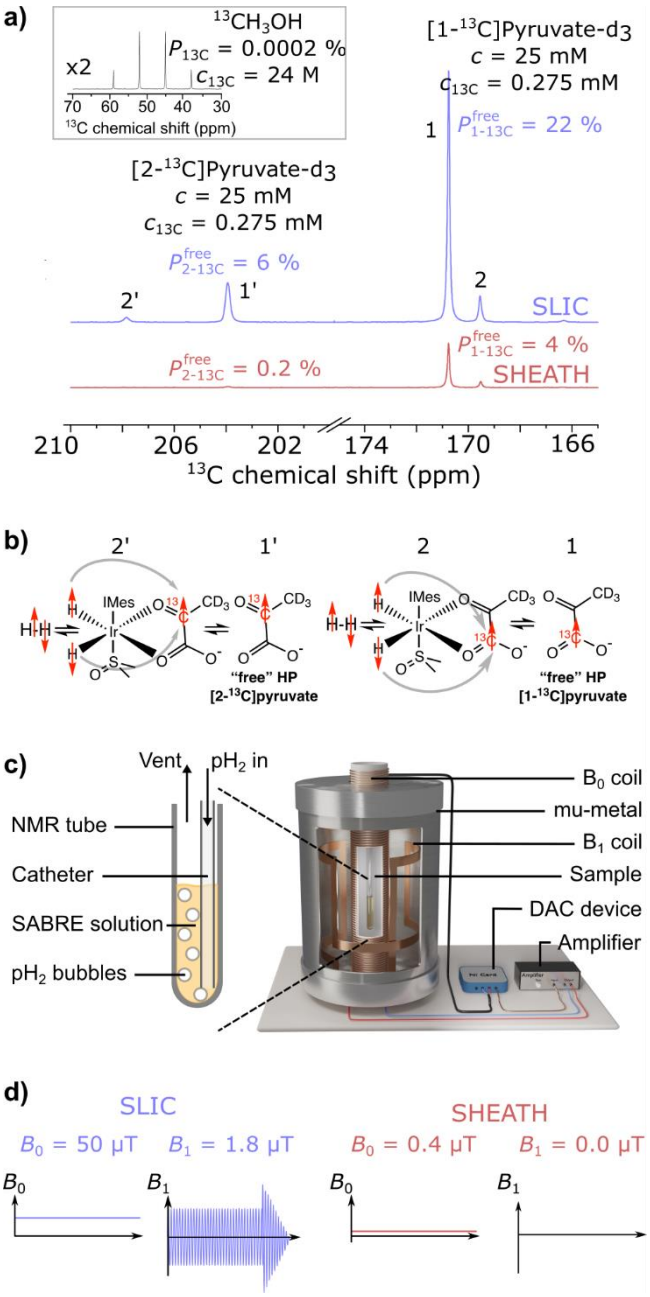

Figure 1. a) ^{13}C NMR spectra of SLIC-SABRE and SABRE-SHEATH hyperpolarization of [1-^{13}C] and [2-^{13}C]pyruvate-d_3; the inset displays the ^{13}C NMR reference spectrum of a ^{13}C-enriched sample of non-hyperpolarized neat methanol. b) The exchange reaction occurring between the Ir-based organometallic complex, free parahydrogen, and free pyruvate in solution. c) The experimental setup used for hyperpolarization experiments keeping the SABRE sample at ~3-7°C, constant magnetic field (B_0), and SLIC radiofrequency field (B_1). A schematic magnification of the NMR tube during parahydrogen (pH_2) bubbling is shown on the left; a rendering of the complete setup is displayed on the right. d) The SLIC-SABRE and SABRE-SHEATH protocols used in this work.

These pyruvate polarization levels are two to six times higher than P_{13C} values reported using SABRE before.[10–13,21] To better understand why SLIC-SABRE at μT fields shows such high efficacy, we carried out experiments using both

protonated and deuterated pyruvate and using SLIC-SABRE and SABRE-SHEATH. The ^{13}C polarization levels are shown in Fig. 2a. Protonated [1-^{13}C] and [2-^{13}C]pyruvate show similar P_{13C} values for both polarization protocols: 12% versus 9% for [1-^{13}C], and 2% in both cases for [2-^{13}C]pyruvate. However, we found that SLIC-SABRE performed much better for pyruvate-d_3: P_{13C} using SABRE-SHEATH (at 0.4μT) was 4% and 0.2% for [1-^{13}C]- and [2-^{13}C]pyruvate-d_3, respectively, but increased to 22% and 6% with SLIC-SABRE.

The rationale behind these observations is that the deuterium nuclei have two distinct effects on relaxation. Firstly, at ultralow fields the deuterons are strongly coupled to the ^{13}C spins and act as a quadrupolar relaxation sink.[17] This is the case during SABRE-SHEATH, and is particularly detrimental for the C2 carbon which has stronger J-couplings to the deuterons than C1. Their second effect is to reduce the rate of intramolecular dipole-dipole relaxation experienced by the ^{13}C spins since the magnetic moments of deuterons are smaller than the ones of protons. This effect manifests in the higher ^{13}C polarizations and more favorable polarization build-up kinetics, which are shown in Fig. 2b. To support this hypothesis, we also present measured T_1 and $T_{1\rho}$ values and find that $T_{1\rho}$ at 50μT is longer than T_1 at 0.4μT for all investigated pyruvate isotopologues (Fig. 2c) ultimately enabling effective polarization build up. Thus, for the pyruvate-d_3 isotopologues for which T_1 under SABRE-SHEATH and $T_{1\rho}$ under SLIC-SABRE conditions differ most, much higher polarizations are achieved with SLIC-SABRE. We envision that further analysis of the polarization transfer in the SABRE exchange complex during SLIC and experimental parameter optimization (mostly reaction temperature, static magnetic field, and SLIC rf field) will enable even greater signal enhancements.

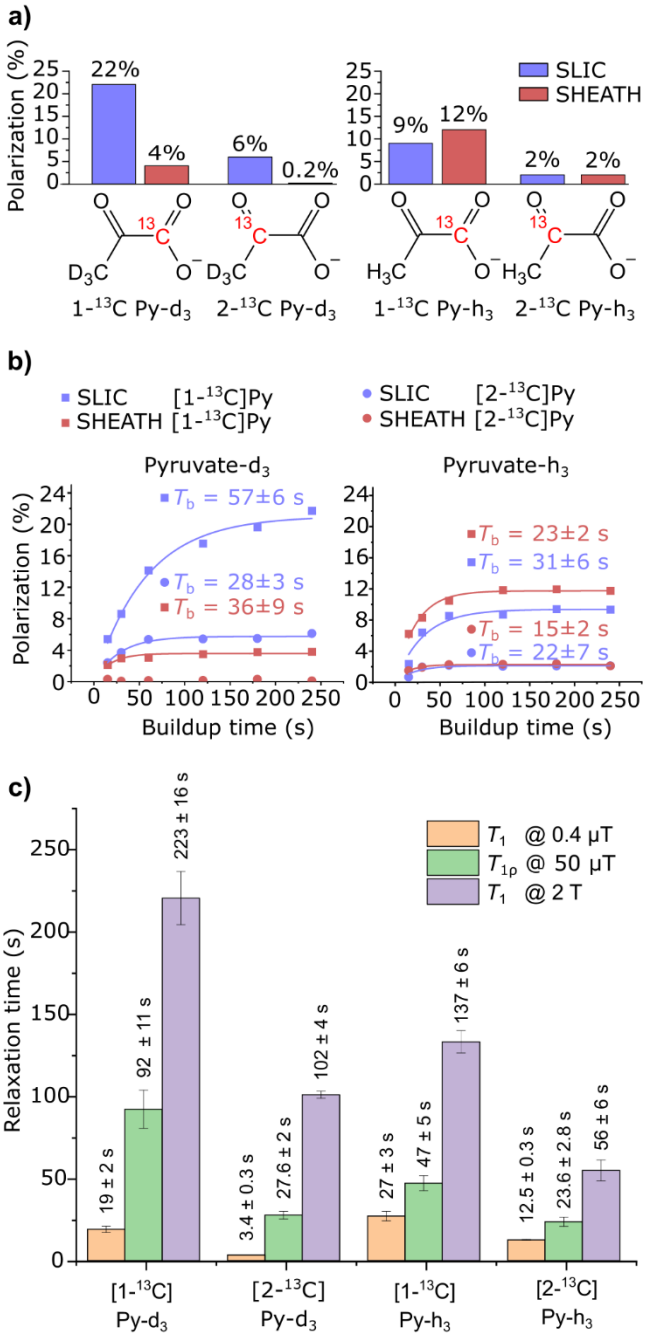

Figure 2. a) SLIC-SABRE and SABRE-SHEATH hyperpolarization yield of [1-^{13}C]pyruvate-d_3 (Py-d_3), [2-^{13}C]Py-d_3, [1-^{13}C]pyruvate (Py-h_3) and [2-^{13}C]Py-h_3. b) Polarization build-up dynamics of SLIC-SABRE and SABRE-SHEATH. c) Relevant relaxation times of ^{13}C hyperpolarization under SABRE-SHEATH conditions at 0.4 μT (T_1), SLIC-SABRE conditions at 50μT ($T_{1\rho}$), and T_1 at the NMR detection field of 1.9T. Relaxation measurements were performed at room temperature; detailed relaxation data is presented in Figs. S6 and S7.

Notably, deuterium isotope labelling can prolong T_1 relaxation also at clinical magnetic fields.[30] In Fig. 2c we show ^{13}C T_1 relaxation values for HP [1-^{13}C] and [2-^{13}C]pyruvate-d_3 measured in CD_3OD at 1.9 T and ambient temperature. We find C1 → 223±16s and C2 → 102±4s versus C1 → 137±6s and C2→56±6s for the deuterated and pronated forms, respectively.

The longer polarization lifetime gained by deuteration will be conducive to yielding high P_{13C} after purification, quality assurance, and injection of the HP contrast agent solution. Importantly, no deuterium isotope effect on metabolic conversion kinetics has been observed for pyruvate,[31] meaning that for metabolic HP MRI pyruvate-d_3 can successfully be used instead of non-deuterated pyruvate. Notably, both isotope-enriched [1-^{13}C]- and [2-^{13}C]pyruvate-d_3 are commercially available and no further chemical modification is needed for SABRE in sharp contrast to hydrogenative pH_2-based hyperpolarization approaches that require suitable unsaturated molecular precursors.[6,7] Additionally, due to the low cost and simplicity of SABRE hardware, this approach can be widely available to researchers. Considering recent advances on rapidly extracting SABRE HP pyruvate from methanol into catalyst-free aqueous solution,[13] the first preclinical metabolic MRI studies using this technique appear on the near horizon.

In conclusion, we have presented an efficient and rapid approach using radiofrequency SLIC and static microtesla fields to produce ^{13}C-hyperpolarized pyruvate using SABRE. While P_{13C} for both C1 and C2 in protonated pyruvate were similar to levels reached with SABRE-SHEATH, SLIC performed substantially better for the deuterated isotopologue pyruvate-d_3, yielding P_{13C} = 22% for C1 and P_{13C} = 6% for C2. These polarizations are approximately 2 and 6 times higher than those previously reported for protonated SABRE-polarized [1-^{13}C]- and [2-^{13}C]pyruvate. We attribute this improvement to deuteration reducing the degree of intramolecular dipole-dipole relaxation, which prolongs the ^{13}C polarization lifetimes. This strategy is made possible with SLIC, since the microtesla fields employed prevent the deuterons from strongly coupling to the ^{13}C nuclei and acting as a quadrupolar relaxation sink. This is an important observation that we envision adapting to other deuterated compounds to widen the portfolio of SABRE-polarized agents or to enhance their polarization levels.

We have demonstrated this technique for pyruvate, a key metabolite and the most-promising HP MRI agent known to date. Experimental parameter optimization may improve the SLIC-SABRE polarizations even further. Both the pyruvate concentration and polarization levels achieved here are sufficient for biomedical applications, and the prolonged polarization lifetimes are promising.[7] We expect this approach to have an important impact on preclinical HP MRI with pyruvate-d_3, facilitating more widespread research and applications.

Acknowledgements

Research reported in this publication was supported by the German Federal Ministry of Education and Research (BMBF) in the funding program “Quantum Technologies – from Basic Research to Market” under the project “QuE-MRT” (contract number: 13N16448), the German Cancer Consortium (DKTK), B.E.S.T. Fluidsysteme GmbH I Swagelok Stuttgart, and the German Research Foundation (DFG #SCHM 3694/1-1, #SCHM 3694/2-1, #SFB1479). This project has received funding from the European Union’s Horizon 2020 Research and Innovation Programme under the Marie Skłodowska-Curie Grant Agreement 101063517. EYC thanks NSF CHE-1904780. ABS and EYC thank Wayne State University for a Postdoctoral Fellow award.

Keywords: parahydrogen • hyperpolarization • SABRE• carbon-13 • pyruvate

[1] Z. J. Wang, M. A. Ohliger, P. E. Larson, J. W. Gordon, R. A. Bok, J. Slater, J. E. Villanueva-Meyer, C. P. Hess, J. Kurhanewicz, D. B. Vigneron, *Radiology* **2019**, *291*, 273.

[2] R. Chowdhury, C. A. Mueller, L. Smith, F. Gong, M.-V. Papoutsaki, H. Rogers, T. Syer, S. Singh, G. Brembilla, A. Retter, M. Bullock, L. Caselton, M. Mathew, E. Dineen, T. Parry, J. Hennig, D. von Elverfeldt, A. B. Schmidt, J.-B. Hövener, M. Emberton, D. Atkinson, A. Bainbridge, D. G. Gadian, S. Punwani, *J. Magn. Reson. Imaging* **n.d.**, *n/a*, DOI 10.1002/jmri.28467.

[3] J. G. Skinner, L. Menichetti, A. Flori, A. Dost, A. B. Schmidt, M. Plaumann, F. A. Gallagher, J.-B. Hövener, *Mol. Imaging Biol.* **2018**, *20*, 902–918.

[4] B. T. Chung, H.-Y. Chen, J. Gordon, D. Mammoli, R. Sriram, A. W. Autry, L. M. Le Page, M. M. Chaumeil, P. Shin, J. Slater, C. T. Tan, C. Suszczynski, S. Chang, Y. Li, R. A. Bok, S. M. Ronen, P. E. Z. Larson, J. Kurhanewicz, D. B. Vigneron, *J. Magn. Reson.* **2019**, *309*, 106617.

[5] J. H. Ardenkjær-Larsen, B. Fridlund, A. Gram, G. Hansson, L. Hansson, M. H. Lerche, R. Servin, M. Thaning, K. Golman, *Proc. Natl. Acad. Sci.* **2003**, *100*, 10158–10163.

[6] A. B. Schmidt, C. R. Bowers, K. Buckenmaier, E. Y. Chekmenev, H. de Maissin, J. Eills, F. Ellermann, S. Glöggler, J. W. Gordon, S. Knecht, I. V. Koptyug, J. Kuhn, A. N. Pravdivtsev, F. Reineri, T. Theis, K. Them, J.-B. Hövener, *Anal. Chem.* **2022**, *94*, 479–502.

[7] J.-B. Hövener, A. N. Pravdivtsev, B. Kidd, C. R. Bowers, S. Glöggler, K. V. Kovtunov, M. Plaumann, R. Katz-Brull, K. Buckenmaier, A. Jerschow, F. Reineri, T. Theis, R. V. Shchepin, S. Wagner, P. Bhattacharya, N. M. Zacharias, E. Y. Chekmenev, *Angew. Chem. Int. Ed.* **2018**, *57*, 11140–11162.

[8] R. W. Adams, J. A. Aguilar, K. D. Atkinson, M. J. Cowley, P. I. P. Elliott, S. B. Duckett, G. G. R. Green, I. G. Khazal, J. López-Serrano, D. C. Williamson, *Science* **2009**, *323*, 1708–1711.

[9] M. J. Cowley, R. W. Adams, K. D. Atkinson, M. C. R. Cockett, S. B. Duckett, G. G. R. Green, J. A. B. Lohman, R. Kerssebaum, D. Kilgour, R. E. Mewis, *J. Am. Chem. Soc.* **2011**, *133*, 6134–6137.

[10] W. Iali, S. S. Roy, B. J. Tickner, F. Ahwal, A. J. Kennerley, S. B. Duckett, *Angew. Chem.* **2019**, *131*, 10377–10381.

[11] P. TomHon, M. Abdulmojeed, I. Adelabu, S. Nantogma, M. S. H. Kabir, S. Lehmkuhl, E. Y. Chekmenev, T. Theis, *J. Am. Chem. Soc.* **2022**, *144*, 282–287.

[12] I. Adelabu, P. TomHon, M. S. H. Kabir, S. Nantogma, M. Abdulmojeed, I. Mandzhieva, J. Ettedgui, R. E. Swenson, M. C. Krishna, T. Theis, B. M. Goodson, E. Y. Chekmenev, *ChemPhysChem* **2022**, *23*, e202100839.

[13] A. B. Schmidt, H. de Maissin, I. Adelabu, S. Nantogma, J. Ettedgui, P. TomHon, B. M. Goodson, T. Theis, E. Y. Chekmenev, *ACS Sens.* **2022**, *7*, 3430–3439.

[14] K. L. Ivanov, A. N. Pravdivtsev, A. V. Yurkovskaya, H.-M. Vieth, R. Kaptein, *Prog. Nucl. Magn. Reson. Spectrosc.* **2014**, *81*, 1–36.

[15] T. Theis, M. L. Truong, A. M. Coffey, R. V. Shchepin, K. W. Waddell, F. Shi, B. M. Goodson, W. S. Warren, E. Y. Chekmenev, *J. Am. Chem. Soc.* **2015**, *137*, 1404–1407.

[16] V. V. Zhivonitko, I. V. Skovpin, I. V. Koptyug, *Chem. Commun.* **2015**, *51*, 2506–2509.

[17] D. A. Barskiy, R. V. Shchepin, C. P. N. Tanner, J. F. P. Colell, B. M. Goodson, T. Theis, W. S. Warren, E. Y. Chekmenev, *ChemPhysChem* **2017**, *18*, 1493–1498.

[18] J. R. Lindale, S. L. Eriksson, C. P. N. Tanner, Z. Zhou, J. F. P. Colell, G. Zhang, J. Bae, E. Y. Chekmenev, T. Theis, W. S. Warren, *Nat. Commun.* **2019**, *10*, 395.

[19] A. N. Pravdivtsev, N. Kempf, M. Plaumann, J. Bernarding, K. Scheffler, J.-B. Hövener, K. Buckenmaier, *ChemPhysChem* **2021**, *22*, 2381–2386.

[20] S. L. Eriksson, J. R. Lindale, X. Li, W. S. Warren, *Sci. Adv.* **2022**, *8*, eabl3708.

[21] S. Nantogma, S. L. Eriksson, I. Adelabu, I. Mandzhieva, A. Browning, P. TomHon, W. S. Warren, T. Theis, B. M. Goodson, E. Y. Chekmenev, *J. Phys. Chem. A* **2022**, *126*, 9114–9123.
[22] A. N. Pravdivtsev, A. V. Yurkovskaya, H. Zimmermann, H.-M. Vieth, K. L. Ivanov, *Chem. Phys. Lett.* **2016**, *661*, 77–82.
[23] S. Knecht, A. S. Kiryutin, A. V. Yurkovskaya, K. L. Ivanov, *J. Magn. Reson.* **2018**, *287*, 10–14.
[24] S. J. DeVience, R. L. Walsworth, M. S. Rosen, *Phys. Rev. Lett.* **2013**, *111*, 173002.
[25] T. Theis, M. Truong, A. M. Coffey, E. Y. Chekmenev, W. S. Warren, *J. Magn. Reson.* **2014**, *248*, 23–26.
[26] A. N. Pravdivtsev, I. V. Skovpin, A. I. Svyatova, N. V. Chukanov, L. M. Kovtunova, V. I. Bukhtiyarov, E. Y. Chekmenev, K. V. Kovtunov, I. V. Koptyug, J.-B. Hövener, *J. Phys. Chem. A* **2018**, *122*, 9107–9114.
[27] S. Knecht, A. S. Kiryutin, A. V. Yurkovskaya, K. L. Ivanov, *Mol. Phys.* **2019**, *117*, 2762–2771.
[28] A. Svyatova, I. V. Skovpin, N. V. Chukanov, K. V. Kovtunov, E. Y. Chekmenev, A. N. Pravdivtsev, J.-B. Hövener, I. V. Koptyug, *Chem. – Eur. J.* **2019**, *25*, 8465–8470.
[29] S. Berner, A. B. Schmidt, M. Zimmermann, A. N. Pravdivtsev, S. Glöggler, J. Hennig, D. von Elverfeldt, J.-B. Hövener, *ChemistryOpen* **2019**, *8*, 728–736.
[30] C. Taglang, D. E. Korenchan, C. von Morze, J. Yu, C. Najac, S. Wang, J. E. Blecha, S. Subramaniam, R. Bok, H. F. VanBrocklin, D. B. Vigneron, S. M. Ronen, R. Sriram, J. Kurhanewicz, D. M. Wilson, R. R. Flavell, *Chem. Commun.* **2018**, *54*, 5233–5236.
[31] A. M. Funk, X. Wen, T. Hever, N. R. Maptue, C. Khemtong, A. D. Sherry, C. R. Malloy, *J. Magn. Reson.* **2019**, *301*, 102–108.